Acta Mech 224, 1849–1864 (2013)
DOI 10.1007/s00707-013-0835-0

K. Asemi · H. Ashrafi · M. Salehi · M. Shariyat

Three-dimensional static and dynamic analysis of functionally graded elliptical plates, employing graded finite elements

Received: 29 October 2012 / Revised: 17 January 2013 / Published online: 24 March 2013

Abstract On the basis of the three-dimensional theory of elasticity, a graded finite element method capable of modeling static and dynamic behaviors of elliptical plates made of functionally graded materials (FGMs) subjected to uniform pressure is developed. In the present paper, two different material properties distributions are considered. For the dynamic analysis, the effective through-the-thickness continuous material properties distribution of the FGM (which is assumed to be composed of ceramic and metallic constituents) is determined based on Mori–Tanaka homogenization technique. The three-dimensional graded finite element formulation is derived based on the principle of minimum potential energy and Rayleigh Ritz method. To solve the time-dependent equations, Newmark's direct integration method is employed. To present the efficiency of the present work, several numerical examples are included. Since similar results are not available in the literature, results of the present formulations are verified by comparing them with available ones of a homogenous elliptical plate.

1 Introduction

A new category of composite materials known as functionally graded materials (FGMs) has given significant attention in recent years. An FGM is a composite material fabricated from two or more constituent phases with a defined composition [1,2]. Unlike the traditional composites which are piecewise homogeneous mixtures or layered structures, material properties of an FGM are affected by those of all constituent materials, so that mechanical properties of the FGMs can be monitored to vary continuously throughout the structure. An FGM can be customized to an application by specifying the form of the gradation function of the material properties, to fit the design requirements. The FGMs can be ideal in applications where the operating conditions are severe, for example, in heat engine components or rocket heat shields. Different closed-form and approximate solutions have been proposed so far for structures with spatially varying material properties [3–11]. However, full utilization of the FGM structures potential requires development of new, accurate, and more adequate modeling techniques. This evidence is generally due to the mathematical complexities that accompany the FGM models when deriving exact solutions for various physical problems. Many researchers have modeled continuous variations of the material properties in the FGM structures by dividing the structure into slices or substructures with isotropic material properties [12,13]. It is evident that this

K. Asemi · M. Salehi
Department of Mechanical Engineering, Amirkabir University of Technology, Tehran, Iran

H. Ashrafi (✉) · M. Shariyat
Department of Mechanical Engineering, K.N. Toosi University of Technology, Tehran, Iran
Tel.: +98-912-8051694
Fax: +98-886-74748
E-mail: hhashrafi@gmail.com

type of modeling leads to approximate rather than accurate global results and unreliable local (such as stress) results.

Plates have been used in various configurations in the engineering structures. Hence, it is important to investigate responses of the functionally graded plates to optimize their resistance against mechanical failures. Mechanical responses of the plate-type structures under mechanical loads have generally been studied for limited (simplest) configurations, that is, rectangular [14] and circular plates [15]. However, elliptical plates have been employed in many engineering structures, (e.g., as flat heads of the fluid carrying tankers).

The elliptical plates are inherently three-dimensional structures, but often have been treated by the two-dimensional plate theories. Several two- [16] and three-dimensional [17] theories are available for analyzing the nonhomogeneous structures. Since variations of the transverse displacement and transverse normal and shear stress components are discarded in the traditional equivalent single-layer plate theories (that are the bases for the shell or plate element of the commercial finite element softwares). Many researchers have attempted to develop closed-form solutions for homogeneous elliptical plates [18–25]. Yüce and Wang [25] determined fundamental natural frequencies of moderately elliptic plates with concentric circular cores analytically, using a boundary perturbation method.

However, since analytical methods can only be successfully applied to structural analyses of plates with very simple geometrical and loading conditions, employing the numerical methods is inevitable for more complex situations. Due to difficulties in obtaining analytical solutions for dynamic responses of the graded elliptical plates, many researchers have focused on static analyses. A closed-form solution was obtained for thermomechanical deformations of a clamped FGM elliptic plate by Cheng and Batra [17]. Lee et al. [26] presented an optimization method based on a genetic algorithm for the homogenous elliptical plates. Hsieh and Lee [27] dealt with the inverse problem of an FGM elliptical plate with large deflections and disturbed boundary under uniform loads based on the classical plate theory and nonlinear von Karman kinematic relations. Chakraverty et al. [28] studied the effects of the inhomogeneity of the material of a plate on the natural frequencies using Gram–Schmidt technique in the Rayleigh Ritz method. Ceribasi et al. [29] analyzed the static behavior of clamped homogeneous Kirchhoff super elliptical plates under uniformly distributed surface loads, using Galerkin's method. A double side approach combining the mathematical programming and the subdomain method in the form of the weighted residuals is presented by Tang et al. [30] for analyzing the deflection of clamped elliptical plates. Ceribasi [31] investigated the elliptical FGM plates using Kirchhoff's assumptions and the meshless approximate method for the solution of the governing equations of the plate. The finite element (FE) technique has been the most powerful and reliable tool for analyzing the FGM structures in recent years. The majority of the published works on FGM plates have been presented based on the conventional finite element techniques [32–36]. However, these methods were based on the classical, first-order and third-order shear deformation plate theories. Kim and Paulino [37], and Zhang and Paulino [38] developed a graded FE approach for modeling the nonhomogeneous structures. They compared the results of the graded versus conventional homogeneous elements under various loading conditions. In these studies, it was shown that the conventional FE formulations cause a discontinuous stress field in the direction perpendicular to the material property gradation, while the graded elements gave a continuous and smooth variation. Ashrafi et al. [39] presented a comparative study between graded finite element and boundary element formulations capable of modeling nonhomogeneous behaviors of the FGM structures.

To the best knowledge of the authors, there are no studies available in the literature on considering the effects of the material nonhomogeneity of the FGM elliptical plates based on the graded elements. The present study is aimed to develop a numerical approach for the FGM elliptical plates based on the three-dimensional theory of elasticity. The governing equations are derived based on the principle of minimum potential energy and Rayleigh Ritz method. In this regard, variations of the material properties are interpolated using general shape functions. By using the three-dimensional graded elements for the analysis of the elliptical plates, discontinuities of the stress distribution, which are present in the conventional FE results, are eliminated. Two different material distributions are used to investigate the static and dynamic behaviors of the FGM elliptical plates. For the static analysis, material properties are considered to vary through-the-thickness direction according to an exponential law. For the dynamic analysis, variations of the volume fractions through the thickness are assumed to obey a power law function. In this case, the effective material properties at each point are determined by the Mori–Tanaka scheme. To solve the time-dependent equations, Newmark's numerical integration method is used.

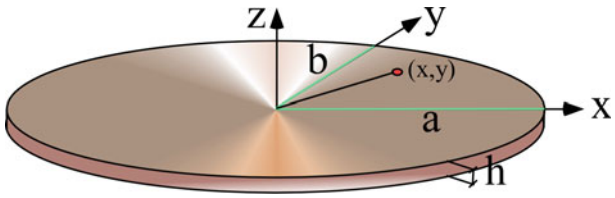

Fig. 1 Geometric parameters of the elliptical FGM plate

2 The governing equations

2.1 Description of variations of the material properties

Consider the elliptic FGM plate shown in Fig. 1. According to the adopted rectangular Cartesian coordinate system, the coordinates vary within the $(-a < x \leq a)$, $(-b < y \leq b)$, and $(0 < z \leq h)$ intervals where a and b are the semimajor and semiminor axes of the elliptical plate. The plate is subjected to a uniform pressure on its upper surface, while its lower surface is free of tractions.

Two different material distributions are used. For the static analysis, a functionally graded material whose material properties vary through-the-thickness direction according to an exponential law is considered,

$$E = E_0 \exp\left(\left(\frac{h-z}{h}\right)^n\right) \tag{1}$$

where n is the material gradient parameter and E_0 is Young's modulus of the upper surface of the plate.

For the dynamic analyses, it is assumed that the FGM plate is made of two randomly distributed isotropic phases and the composition of the FGM varies only in the thickness direction. The volume fraction of ceramic and metal is given by

$$V_{\mathrm{m}} = 1 - \left(\frac{z}{h}\right)^n \tag{2.1}$$

$$V_{\mathrm{c}} = 1 - V_{\mathrm{m}} \tag{2.2}$$

where n is a nonnegative volume fraction exponent and the subscripts c and m stand, respectively, for the ceramic and the metal.

Mori–Tanaka homogenization method [40] is used to determine the effective properties at each point. According to the Mori–Tanaka homogenization method, the effective bulk modulus (K) and the effective shear modulus (G) of the FGM elliptic plate are given by [40]

$$\frac{K - K_{\mathrm{c}}}{K_{\mathrm{m}} - K_{\mathrm{c}}} = \frac{V_{\mathrm{m}}}{1 + \frac{(1-V_{\mathrm{m}})(K_{\mathrm{m}}-K_{\mathrm{c}})}{K_{\mathrm{c}}+\frac{4}{3}G_{\mathrm{c}}}}, \tag{3}$$

$$\frac{G - G_{\mathrm{c}}}{G_{\mathrm{m}} - G_{\mathrm{c}}} = \frac{V_{\mathrm{m}}}{1 + \frac{(1-V_{\mathrm{m}})(G_{\mathrm{m}}-G_{\mathrm{c}})}{G_{\mathrm{c}}+f_{\mathrm{c}}}} \tag{4}$$

where

$$f_{\mathrm{c}} = \frac{G_{\mathrm{c}}\,(9K_{\mathrm{c}} + 8G_{\mathrm{c}})}{6\,(K_{\mathrm{c}} + 2G_{\mathrm{c}})}. \tag{5}$$

The effective values of the modulus of elasticity and Poisson's ratio of the structure are found from

$$E = \frac{9KG}{3K + G}, \tag{6}$$

$$\nu = \frac{3K - 2G}{2(3K + G)}. \tag{7}$$

According to these distributions, the bottom surface of the FGM plate is pure metallic, the top surface is pure ceramic, and different volume fractions of the constituent materials can be obtained for different values of n. However, the effective mass density of the FGM plate may be determined by the rule of mixtures.

2.2 Equations of motion

In the absence of the body forces, the equations of motion for an FGM elliptic plate can be written as follows:

$$\frac{\partial \sigma_{xx}}{\partial x} + \frac{\partial \sigma_{xy}}{\partial y} + \frac{\partial \sigma_{zx}}{\partial z} = \rho(z)\frac{\partial^2 u}{\partial t^2}, \tag{8.1}$$

$$\frac{\partial \sigma_{xy}}{\partial x} + \frac{\partial \sigma_{yy}}{\partial y} + \frac{\partial \sigma_{yz}}{\partial z} = \rho(z)\frac{\partial^2 v}{\partial t^2}, \tag{8.2}$$

$$\frac{\partial \sigma_{zx}}{\partial x} + \frac{\partial \sigma_{yz}}{\partial y} + \frac{\partial \sigma_{zz}}{\partial z} = \rho(z)\frac{\partial^2 w}{\partial t^2} \tag{8.3}$$

where ρ is the mass density which depends on z coordinate. u, v and w are the displacement components along the x, y and z axes, respectively, and $\sigma_{ij}(i, j = x, y, z)$ are the stress components.

2.3 Stress–strain relationships

The stress–strain relationships of the linear elasticity may be written based on Hooke's generalized law as follows [41]:

$$\boldsymbol{\sigma} = \mathbf{D}\boldsymbol{\varepsilon} \tag{9}$$

in which

$$\boldsymbol{\sigma} = \left\{\sigma_{xx} \quad \sigma_{yy} \quad \sigma_{zz} \quad \sigma_{xy} \quad \sigma_{yz} \quad \sigma_{zx}\right\}^{\mathrm{T}}, \tag{10}$$

$$\boldsymbol{\varepsilon} = \left\{\varepsilon_{xx} \quad \varepsilon_{yy} \quad \varepsilon_{zz} \quad \varepsilon_{xy} \quad \varepsilon_{yz} \quad \varepsilon_{zx}\right\}^{\mathrm{T}}, \tag{11}$$

$$\begin{aligned}\mathbf{D} &= \frac{E(z)(1-\nu)}{(1+\nu)(1-2\nu)}\begin{pmatrix} 1 & \frac{\nu}{1-\nu} & \frac{\nu}{1-\nu} & 0 & 0 & 0 \\ \frac{\nu}{1-\nu} & 1 & \frac{\nu}{1-\nu} & 0 & 0 & 0 \\ \frac{\nu}{1-\nu} & \frac{\nu}{1-\nu} & 1 & 0 & 0 & 0 \\ 0 & 0 & 0 & \frac{1-2\nu}{2(1-\nu)} & 0 & 0 \\ 0 & 0 & 0 & 0 & \frac{1-2\nu}{2(1-\nu)} & 0 \\ 0 & 0 & 0 & 0 & 0 & \frac{1-2\nu}{2(1-\nu)} \end{pmatrix} \\ &= E(z)\boldsymbol{\Lambda}\end{aligned} \tag{12}$$

where $\boldsymbol{D}$ is the elastic coefficients matrix. It is assumed that the elasticity modulus E varies in the z direction while Poisson's ratio ν is constant. The constant part of matrix $\boldsymbol{D}$ is defined as $\boldsymbol{\Lambda}$.

2.4 Strain–displacement relationships

The strain–displacement relationships of the infinitesimal theory of elasticity in the rectangular Cartesian coordinates are

$$\begin{aligned}&\varepsilon_{xx} = \frac{\partial u}{\partial x}, \quad \varepsilon_{yy} = \frac{\partial v}{\partial y}, \quad \varepsilon_{zz} = \frac{\partial w}{\partial z}, \quad \varepsilon_{xy} = \frac{1}{2}\left(\frac{\partial u}{\partial y} + \frac{\partial v}{\partial x}\right), \\ &\varepsilon_{yz} = \frac{1}{2}\left(\frac{\partial v}{\partial z} + \frac{\partial w}{\partial y}\right), \quad \varepsilon_{zx} = \frac{1}{2}\left(\frac{\partial w}{\partial x} + \frac{\partial u}{\partial z}\right),\end{aligned} \tag{13}$$

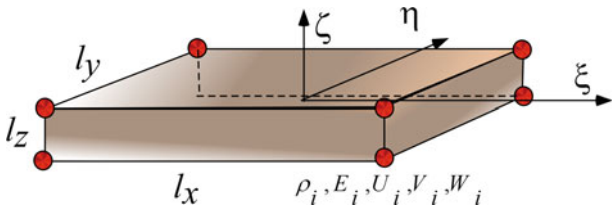

Fig. 2 Nodal degrees of freedom of the ith node of the adopted graded three-dimensional element

The strain–displacement relationships (13) may be written as

$$\boldsymbol{\varepsilon} = \mathbf{dq} \tag{14}$$

where

$$\mathbf{d} = \begin{pmatrix} \frac{\partial}{\partial x} & 0 & 0 \\ 0 & \frac{\partial}{\partial y} & 0 \\ 0 & 0 & \frac{\partial}{\partial z} \\ 1/2\frac{\partial}{\partial y} & 1/2\frac{\partial}{\partial x} & 0 \\ 0 & 1/2\frac{\partial}{\partial z} & 1/2\frac{\partial}{\partial y} \\ 1/2\frac{\partial}{\partial z} & 0 & 1/2\frac{\partial}{\partial x} \end{pmatrix}, \tag{15}$$

$$\mathbf{q} = \begin{Bmatrix} u \\ v \\ w \end{Bmatrix}. \tag{16}$$

For a clamped elliptical plate, the essential boundary condition is

$$u, v, w\left(x^2/a^2 + y^2/b^2 = 1, z\right) = 0. \tag{17}$$

3 Graded finite element modeling

Consider the three-dimensional 8-node linear brick element shown in Fig. 2. As it has been mentioned in the foregoing sections, in contrast to the conventional solid (brick) elements, material properties are among the nodal degrees of freedom (Fig. 2).

Following the common FE approximation, the displacement components vector $\boldsymbol{q}$ of an arbitrary point of the element may be related to the nodal displacement vector of the element $\boldsymbol{\delta}^{(e)}$ through the shape function matrix $\boldsymbol{N}$, where the spatial and time variables are separated as

$$\mathbf{q}(\xi, \eta, \zeta, t) = \mathbf{N}(\xi, \eta, \zeta)\, \boldsymbol{\delta}^{(e)}(t) \tag{18}$$

where

$$\boldsymbol{\delta}^{(e)} = \{U_1 \quad V_1 \quad W_1 \ldots U_8 \quad V_8 \quad W_8\}^{\mathrm{T}}, \tag{19}$$

$$\mathbf{N}(\xi, \eta, \zeta) = \begin{bmatrix} N_1 & 0 & 0 & N_2 & 0 & 0 & N_3 & 0 & 0 & N_4 & 0 & 0 & N_5 & 0 & 0 & N_6 & 0 & 0 & N_7 & 0 & 0 & N_8 & 0 & 0 \\ 0 & N_1 & 0 & 0 & N_2 & 0 & 0 & N_3 & 0 & 0 & N_4 & 0 & 0 & N_5 & 0 & 0 & N_6 & 0 & 0 & N_7 & 0 & 0 & N_8 & 0 \\ 0 & 0 & N_1 & 0 & 0 & N_2 & 0 & 0 & N_3 & 0 & 0 & N_4 & 0 & 0 & N_5 & 0 & 0 & N_6 & 0 & 0 & N_7 & 0 & 0 & N_8 \end{bmatrix}, \tag{20}$$

and the natural coordinates ξ, η, and ζ are along the coordinate axes x, y, and z, respectively. The components of the shape matrix may be expressed in terms of the natural coordinates shown in Fig. 2 as [41]:

$$N_i(\xi, \eta, \zeta) = \frac{1}{8}(1 + \xi_i\xi)(1 + \eta_i\eta)(1 + \zeta_i\zeta) \tag{21}$$

where $(-1 \le \xi \le 1)$, $(-1 \le \eta \le 1)$ and $(-1 \le \zeta \le 1)$.

In addition to the displacement field, the heterogeneity of the material properties of the FGM may also be determined based on their nodal values. This procedure can be used even for multi-directional functionally graded materials. Therefore, a graded finite element method (GFEM) may be used to effectively trace smooth variations of the material properties at the element level. Using the graded elements for the modeling of gradation of the material properties leads to more accurate results than dividing the solution domain into homogenous elements. In this regard, shape functions similar to those of the displacement field may be used:

$$\begin{aligned} E(\zeta) &= \sum_{i=1}^{8} E_i \; N_i\,(\xi,\eta,\zeta) = \widehat{\mathbf{N}}\boldsymbol{\Xi}, \\ \rho(\zeta) &= \sum_{i=1}^{8} \rho_i \; N_i(\xi,\eta,\zeta) = \widehat{\mathbf{N}}\Re \end{aligned} \tag{22}$$

where E_i and ρ_i are the modulus of elasticity and mass density values corresponding to node i (Fig. 2), and $\boldsymbol{\Xi}$ and $\Re$ are, respectively, vectors of the nodal elasticity moduli and mass densities, and

$$\widehat{\mathbf{N}} = \langle N_1 \quad N_2 \ldots N_8 \rangle\,, \boldsymbol{\Xi} = \langle E_1 \quad E_2 \quad \ldots \quad E_8 \rangle^T\,, \Re = \langle \rho_1 \quad \rho_2 \quad \ldots \quad \rho_8 \rangle^T\,. \tag{23}$$

Therefore, Eq. (12) may be rewritten as:

$$\mathbf{D} = \boldsymbol{\Lambda}\left(\widehat{\mathbf{N}}\boldsymbol{\Xi}\right). \tag{24}$$

Substituting (18) into (14) gives the strain matrix of the element (e) as

$$\boldsymbol{\varepsilon}^{(e)} = \mathbf{d}\mathbf{N}\boldsymbol{\delta}^{(e)} = \mathbf{B}\boldsymbol{\delta}^{(e)}. \tag{25}$$

The governing equations of the FE model may be derived based on the principle of minimum potential energy and Rayleigh Ritz method. The total potential energy of the plate may be expressed as

$$\begin{aligned} \Pi^{(e)} &= \frac{1}{2}\int\limits_{V^{(e)}} \left(\boldsymbol{\varepsilon}^{(e)}\right)^T \boldsymbol{\sigma}^{(e)}\mathrm{d}V - \int\limits_{A^{(e)}} (\mathbf{q})^T \mathbf{p}\;\mathrm{d}A + \int\limits_{V^{(e)}} \rho(\mathbf{q})^T \ddot{\mathbf{q}}^{(e)}\mathrm{d}V \\ &= \frac{1}{2}\int\limits_{V^{(e)}} \left(\boldsymbol{\delta}^{(e)}\right)^T \mathbf{B}^T \boldsymbol{\Lambda}\left(\widehat{\mathbf{N}}\boldsymbol{\Xi}\right)\mathbf{B}\boldsymbol{\delta}^{(e)}\mathrm{d}V - \int\limits_{A^{(e)}} \left(\boldsymbol{\delta}^{(e)}\right)^T \mathbf{N}^T \mathbf{p}\;\mathrm{d}A \\ &\quad + \int\limits_{V^{(e)}} \left(\boldsymbol{\delta}^{(e)}\right)^T \mathbf{N}^T \left(\widehat{\mathbf{N}}\Re\right)\mathbf{N}\ddot{\boldsymbol{\delta}}^{(e)}\mathrm{d}V \end{aligned} \tag{26}$$

where $V^{(e)}$ and A are, respectively, volume and area of the element. $\mathbf{p}$ is the traction vector, and the last term of Eq. (26) represents the work of the inertial loads.

Therefore, employing the principle of minimum total potential energy leads to the following result:

$$\begin{aligned} &\frac{\partial \Pi^{(e)}}{\partial\left(\boldsymbol{\delta}^{(e)}\right)^T} = 0 \\ &\Rightarrow \left[\int\limits_{V^{(e)}} \mathbf{N}^T \left(\widehat{\mathbf{N}}\Re\right)\mathbf{N}\mathrm{d}V\right]\ddot{\boldsymbol{\delta}}^{(e)} + \left[\int\limits_{V^{(e)}} \mathbf{B}^T \boldsymbol{\Lambda}\left(\widehat{\mathbf{N}}\boldsymbol{\Xi}\right)\mathbf{B}\mathrm{d}V\right]\boldsymbol{\delta}^{(e)} = \int\limits_{A^{(e)}} \mathbf{N}^T \mathbf{p}\,\mathrm{d}A, \end{aligned} \tag{27}$$

or in a compact form:

$$\mathbf{M}^{(e)}\ddot{\boldsymbol{\delta}}^{(e)} + \mathbf{K}^{(e)}\boldsymbol{\delta}^{(e)} = \mathbf{F}^{(e)} \tag{28}$$

where

$$\mathbf{K}^{(e)} = \int_{V^{(e)}} \mathbf{B}^T \mathbf{\Lambda} \left(\widehat{\mathbf{N}\Xi}\right) \mathbf{B} \mathrm{d}V, \tag{29}$$

$$\mathbf{M}^{(e)} = \int_{V^{(e)}} \mathbf{N}^T \left(\widehat{\mathbf{N}\Re}\right) \mathbf{N} \mathrm{d}V, \tag{30}$$

$$\mathbf{F}^{(e)} = \int_{A^{(e)}} \mathbf{N}^T \mathbf{p} \mathrm{d}A \tag{31}$$

and

$$\mathbf{p} = \begin{Bmatrix} 0 \\ 0 \\ p_z \end{Bmatrix}. \tag{32}$$

Since the plate is subjected to a uniform pressure at its upper surface, the components of the traction vector are equal to zero in the x and y directions. Integrals of the mass and stiffness matrices are evaluated numerically using 8-point Gaussian points and Gauss–Legendre technique [41].

By assembling the element matrices, the governing finite element equations of motion of the FGM elliptic plate will have the following form:

$$\mathbf{M}\ddot{\boldsymbol{\delta}} + \mathbf{K}\boldsymbol{\delta} = \mathbf{F}. \tag{33}$$

Various numerical methods can be employed to solve Eq. (33) in the space and time domains. To solve the equilibrium equation, Newmark's numerical integration method [41] is used. Newmark integration parameters [41] are chosen as: $\gamma = \frac{1}{2}$ and $\beta = \frac{1}{4}$, which lead to a constant average acceleration. This choice of parameters corresponds to the trapezoidal rule which is unconditionally stable in linear analyses. Moreover, to achieve convergent results, the time step is adopted as 2e−6 s.

For static analysis, Eq. (33) reduces to

$$\mathbf{K}\boldsymbol{\delta} = \mathbf{F}. \tag{34}$$

4 Numerical results and discussion

4.1 Static analysis

4.1.1 Verification

The prepared three-dimensional GFEM code for analyzing the FGM elliptic plates can be verified using the results of a homogenous plate obtained by the authors in ANSYS finite element analysis software. The elliptic plate is fully clamped and subjected to a uniform pressure on its upper surface. Parameter values of the loading and the homogenous elliptic plate are:

$$h = 0.2\,\mathrm{m}, \quad E_0 = 70\ \mathrm{GPa}, \quad \nu = 0.3, \quad P = 20\,\mathrm{MPa}.$$

To achieve convergent results in the present study and ANSYS software, about 2,000 solid elements (8-node brick elements) are considered. Through the thickness distribution of the lateral deflection, the central section of the plate is shown in Fig. 3 and compared with ANSYS results. Figure 3 shows a good agreement between the results. These results are obtained for two different ratios of major to minor radii of the elliptic plate, that is, $m = a/b = 2$ and $m = a/b = 3$.

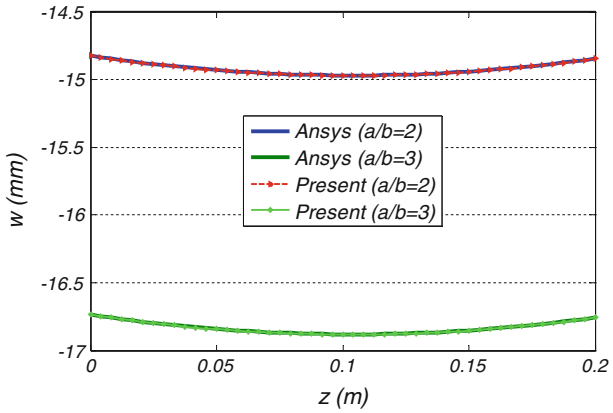

Fig. 3 A comparison between through-the-thickness distributions of the lateral deflection of the central section of the homogenous elliptic plate predicted by present results and ANSYS software

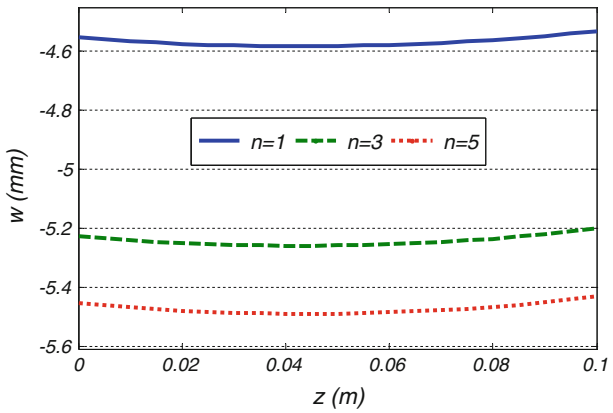

Fig. 4 Through-the-thickness distribution of lateral deflection (w) of the central section of the elliptical plate for different gradation exponents

4.1.2 Numerical results

Consider an FGM elliptical plate with major and minor radii $a = 1$ and $b = 0.5$ m, and thickness $h = 0.1$ m. The material properties vary through the thickness direction according to an exponential material gradation presented in Eq. (1) with $E_0 = 70$ GPa. The plate is subjected to a uniform pressure loading P in the z-direction on its upper surface, while its sides are fully clamped. The static pressure is taken as $P = 20$ MPa. To obtain convergent results, about 2,000 brick elements are considered.

Through-the-thickness distribution of the lateral deflection of the central section of the FGM elliptical plate is shown in Fig. 4 for different gradation exponents $n = 1$, 3, and 5. It is seen from Fig. 4 that the deflections increase as n increases from $n = 1$ to 5. This behavior is due to the resulting decrease in the modulus of elasticity with an increase in the exponent n. Variations of the stress component σ_{zz} at the central section of the FGM elliptical plate in the transverse direction is shown in Fig. 5. Results illustrated in Fig. 5 reveal that the transverse distribution of the stress component σ_{zz} does not change significantly with the gradation exponent n. As it can be readily seen from this figure, the natural boundary conditions of upper and lower surfaces are adequately satisfied.

Distributions of the lateral deflection and the displacement component u of the mid-plane of the elliptical plate are illustrated along the major axis ($y = 0, z = h/2$) in Figs. 6 and 7 for different gradation exponents. Figure 6 shows that the lateral deflection increases by increasing the gradation exponent n. Distributions of the stress components σ_{xx}, σ_{yy}, and σ_{zx} of the mid-plane are depicted in Figs. 8, 9, and 10, respectively, along the major axis of the elliptical FGM plate, for different gradation exponents. Figures 8 and 9 show that the stress components σ_{xx} and σ_{yy} decrease by increasing the heterogeneity exponent n. Furthermore, Fig. 10

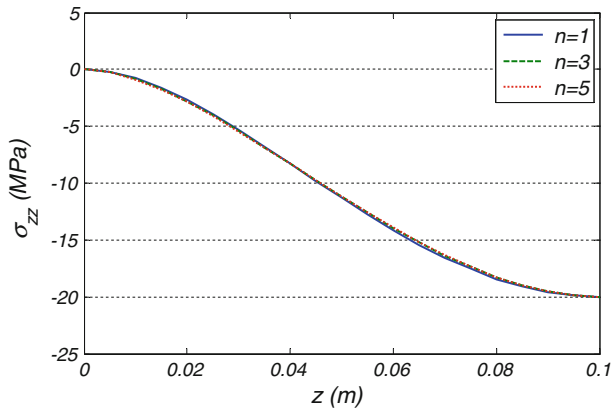

Fig. 5 Through-the-thickness distribution of the stress component (σ_{zz}) of the elliptical plate at the central section for different gradation exponents

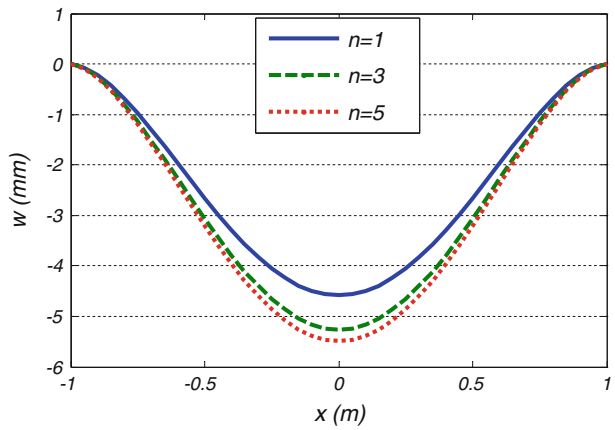

Fig. 6 Distribution of the lateral deflection of the mid-plane, along the major axis of the elliptical plate for different gradation exponents

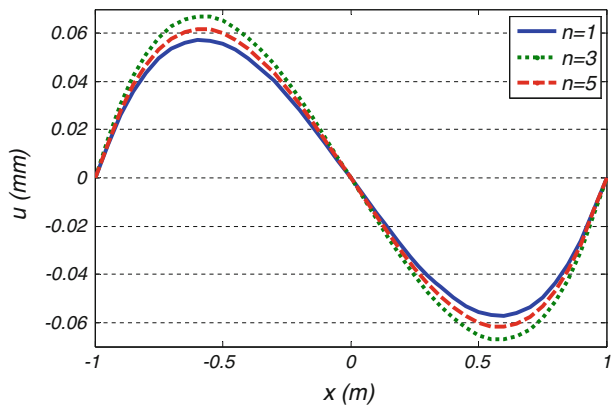

Fig. 7 Distribution of the displacement component (u) of the mid-plane, along the major axis of the elliptical plate for different gradation exponents

illustrates that the distribution of the stress component σ_{zx} does not change significantly with the heterogeneity exponent n.

Distributions of the lateral deflection and the displacement component v of the mid-plane are illustrated in Figs. 11 and 12, respectively, along the minor axis ($x = 0, z = h/2$) of the elliptical FGM plate for different gradation exponents. These results show that the values of the displacement components increase by increasing

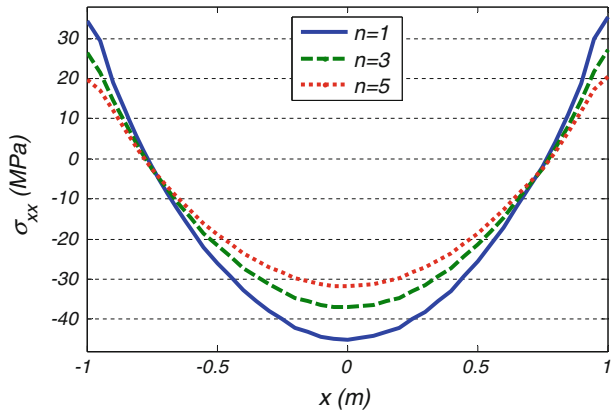

Fig. 8 Distribution of the stress component (σ_{xx}) of the mid-plane, along the major axis of the elliptical plate for different gradation exponents

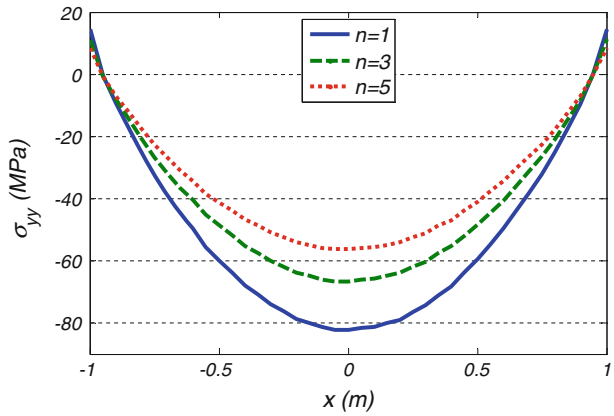

Fig. 9 Distribution of the stress component (σ_{yy}) of the mid-plane, along the major axis of the elliptical plate for different gradation exponents

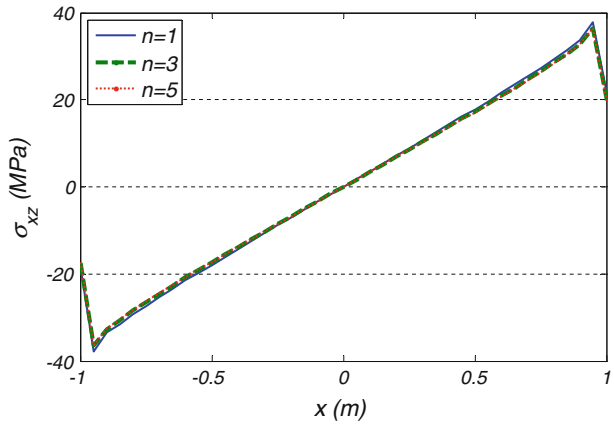

Fig. 10 Distribution of the stress component (σ_{zx}) of the mid-plane, along the major axis of the elliptical plate for different gradation exponents

the heterogeneity exponent n. Although in Fig. 12 similar behaviors are noticed for $n = 1$ and $n = 3$, the resulting behavior for $n = 5$ is different. Indeed, this phenomenon is due to nonlinear behaviors of the material properties.

Distributions of the stress components σ_{xx}, σ_{yy} and σ_{zy} of the mid-plane of the elliptical FGM plate are depicted in Figs. 13, 14, and 15, respectively, along the minor axis for different gradation exponents. Moreover,

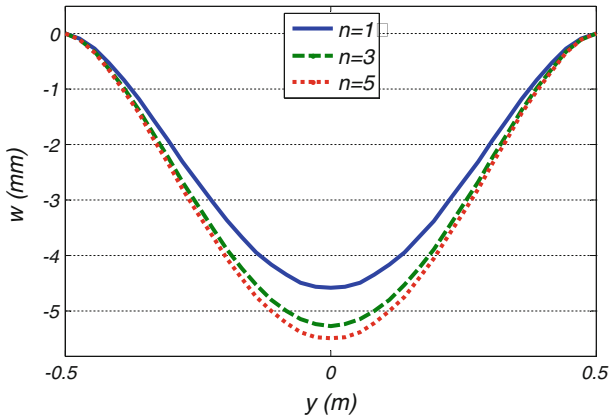

Fig. 11 Distribution of the lateral deflection of the mid-plane, along the minor axis of the elliptical plate for different gradation exponents

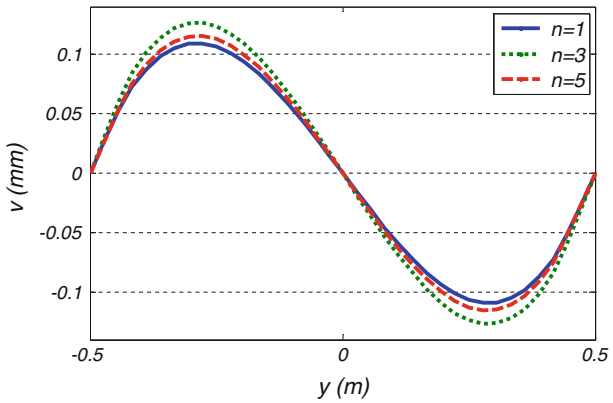

Fig. 12 Distribution of the displacement component (v) of the mid-plane, along the minor axis of the elliptical plate for different gradation exponents

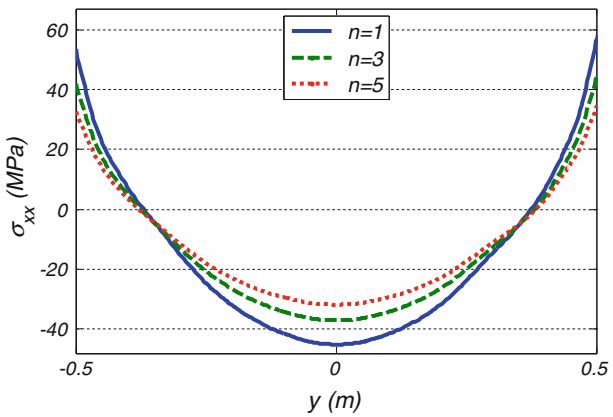

Fig. 13 Distribution of the stress component (σ_{xx}) of the mid-plane, along the minor axis of the elliptical plate for different gradation exponents

Fig. 16 shows the variations of the stress σ_{zz} along the minor axis of the nonhomogeneous elliptical plate for different gradation exponents. As can be seen from the results of the stress components, both the through-the-thickness and longitudinal distributions of the stress components have continuous variations due to using graded elements.

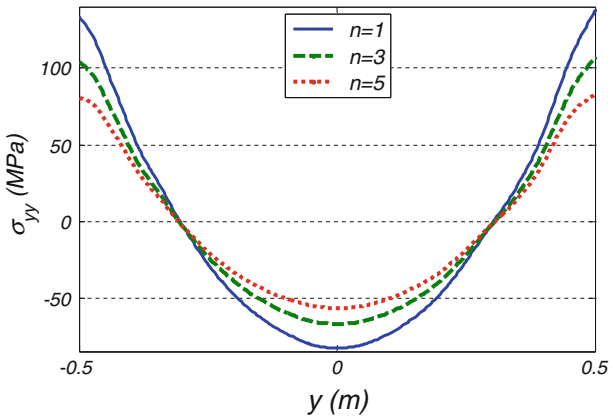

Fig. 14 Distribution of the stress component (σ_{yy}) of the mid-plane, along the minor axis of the elliptical plate for different gradation exponents

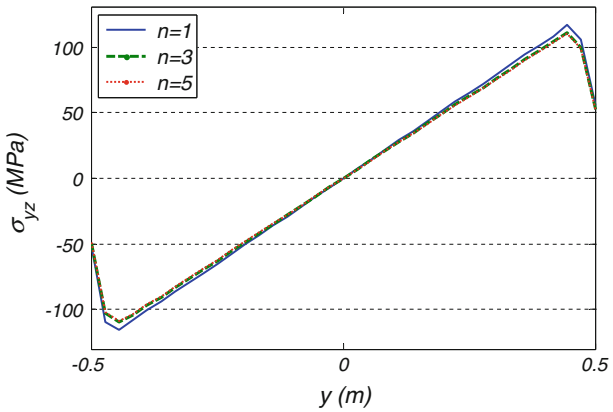

Fig. 15 Distribution of the stress component (σ_{yz}) of the mid-plane, along the minor axis of the elliptical plate for different gradation exponents

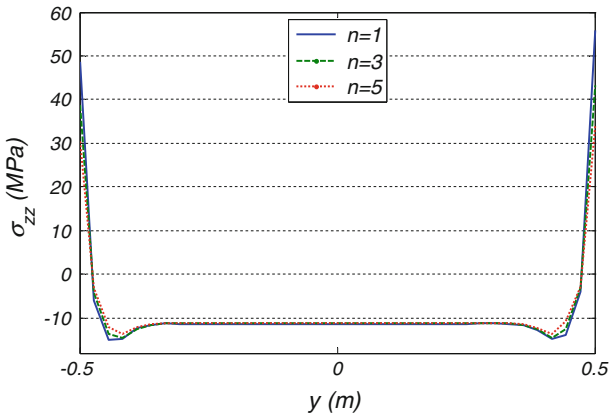

Fig. 16 Distribution of the stress component (σ_{zz}) of the mid-plane, along the minor axis of the elliptical plate for different gradation exponents

4.2 Dynamic analysis

Consider the elliptic FGM plate of the previous section once again. As mentioned before, it is assumed that the FGM plate is fabricated from two randomly distributed isotropic constituent materials. Mori–Tanaka homoge-

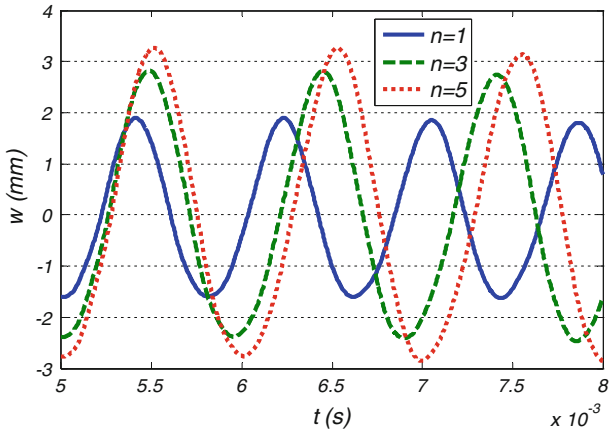

Fig. 17 Time histories of lateral deflection of the center point of an elliptical plate for different gradation exponents

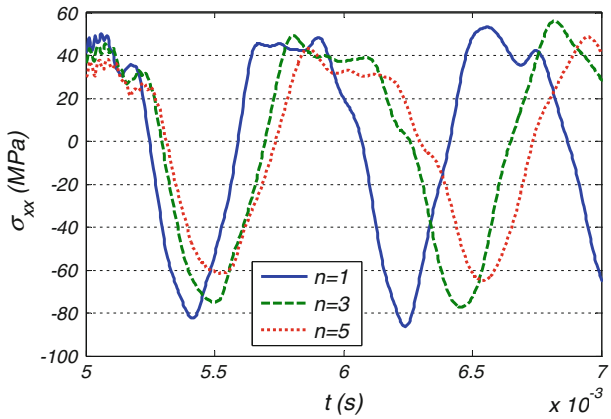

Fig. 18 Time histories of the stress component (σ_{xx}) of the center point of the elliptical plate for different gradation exponents

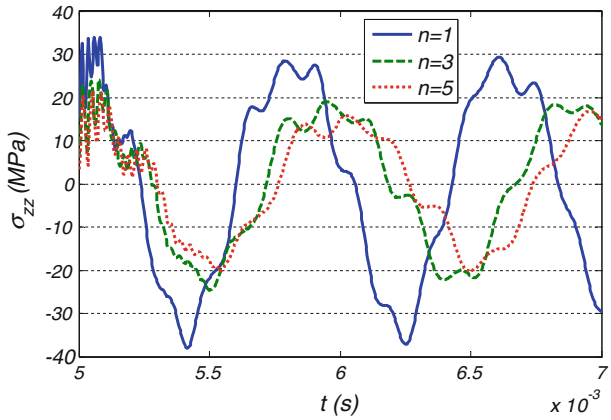

Fig. 19 Time histories of the stress component (σ_{zz}) of the center point of the elliptical plate for different gradation exponents

nization method is used to find the effective properties at each point. The material properties of the constituent materials are assumed to be $E_c = 380\,\text{GPa}$, $\rho_c = 3{,}800\,\text{kg/m}^3$, and $E_m = 70\,\text{GPa}$, $\rho_m = 2{,}707\,\text{kg/m}^3$.

The plate is fully clamped and subjected to a uniformly distributed impact load at its upper surface. The loading function is assumed as

$$p(t) = \begin{cases} p_0 t & t \le 0.005\,\text{s} \\ 0 & t > 0.005\,\text{s} \end{cases}$$

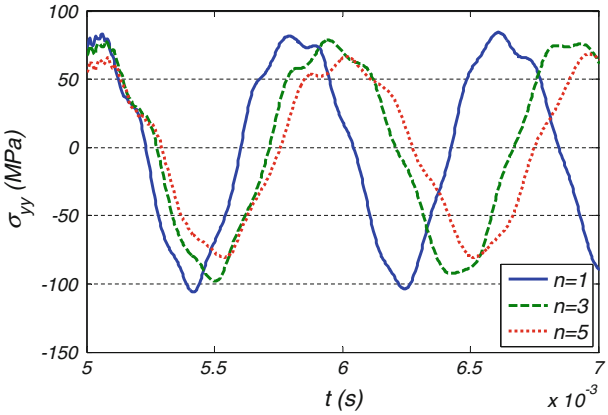

Fig. 20 Time histories of the stress component (σ_{yy}) of the center point of the elliptical plate for different gradation exponents

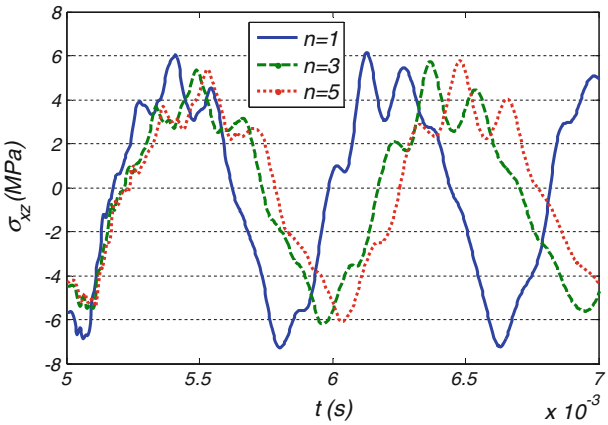

Fig. 21 Time histories of the stress component (σ_{xz}) of the center point of the elliptical plate for different gradation exponents

where p_0 is considered as 4 GPa/s. The plate is unloaded in $t = 0.005$ s. It is obvious that after the unloading a transient vibration which is affected by the wave propagation, reflection, and interference would occur. Results of different values of the power law exponents are presented and discussed in the next paragraphs.

Figure 17 shows the time history of the lateral deflection of the center point ($x = y = 0, z = h/2$) of the elliptical plate after unloading for different gradation exponents. Figure 17 shows that by increasing the gradation exponent the volume fraction of the metallic phase increases and subsequently the amplitude of the vibration increases. Figures 18, 19, 20, and 21 show the time histories of the stress components σ_{xx}, σ_{zz}, σ_{yy}, and σ_{xz} of the center point of the elliptical plate for different gradation exponents, respectively. Results reveal that the propagation of the stress waves following the unloading is strongly affected by the gradation exponent. The obtained results denote that using a graded element has several advantages over using conventional elements in the dynamic and wave propagation analyses. In the conventional FE methods, continuous variations of the material properties are approximated by discrete and homogenous ones. Therefore, adjacent elements may have quite different isotropic material properties. Boundaries of these homogenous elements experience jumps in the material properties, cause artificial wave reflections, and have cumulative effects on magnitude and speed of the stress waves propagation. Therefore, by using the graded elements wherein the material properties vary continuously, improved accuracy may be attained without refining the mesh size.

5 Conclusions

Static and dynamic analyses of the FGM elliptic plate are accomplished in the present research based on the three-dimensional theory of elasticity. Graded elements, the principle of minimum energy, and Rayleigh–Ritz energy method are employed. Newmark's numerical integration method was used to derive time histories of

the displacement and stress components. For the static analysis, it is assumed that material properties vary through-the-thickness direction according to an exponential material gradation, and for the dynamic analyses, the effective material properties distribution of the FGM plate was determined using Mori–Tanaka homogenization technique. The proposed approach is validated through comparing the present results for a fully clamped homogenous elliptical plate with results of ANSYS commercial FE software. The obtained results reveal that the distribution of the mechanical stress components can be modified to meet a specific requirement by selecting an appropriate heterogeneity parameter. Furthermore, results confirm that using graded elements provides smoother and more accurate results than homogeneous elements.

References

1. Miyamoto, Y., Kaysser, W.A., Rabin, B.H.: Functionally Graded Materials: Design, Processing and Applications. Kluwer, Dordrecht (1999)
2. Suresh, S., Mortensen, A.: Functionally Graded Materials. Institute of Materials, IOM Communications, London (1998)
3. Banks-Sills, L., Rami, E., Yuri, B.: Modeling of functionally graded materials in dynamic analyses. Compos. Part B Eng. **33**, 7–15 (2002)
4. Tornabene, F.: Vibration analysis of functionally graded conical, cylindrical and annular shell structures with a four-parameter power-law distribution. Comput. Methods Appl. Mech. Eng. **198**, 2911–2935 (2009)
5. Akbarzadeh, A.H., Abbasi, M., Hosseini Zad, S.K., Eslami, M.R.: Dynamic analysis of functionally graded plates using the hybrid Fourier–Laplace transform under thermo mechanical loading. Meccanica **46**, 1373–1392 (2011)
6. Tornabene, F., Viola, E., Inman, D.J.: 2-D differential quadrature solution for vibration analysis of functionally graded conical, cylindrical and annular shell structures. J. Sound Vib. **328**, 259–290 (2009)
7. Viola, E., Tornabene, F.: Free vibrations of three parameter functionally graded parabolic panels of revolution. Mech. Res. Commun. **36**, 587–594 (2009)
8. Malekzadeh, P., Golbahar Haghighi, M.R., Atashi, M.M.: Free vibration analysis of elastically supported functionally graded annular plates subjected to thermal environment. Meccanica **46**, 893–913 (2011)
9. Tornabene, F., Liverani, A., Caligiana, G.: FGM and laminated doubly curved shells and panels of revolution with a free-form meridian: a 2-D GDQ solution for free vibrations. Int. J. Mech. Sci. **53**, 446–470 (2011)
10. Asemi, K., Salehi, M., Akhlaghi, M.: Elastic solution of a two-dimensional functionally graded thick truncated cone with finite length under hydrostatic combined loads. Acta Mech. **217**, 119–134 (2011)
11. Shariyat, M., Alipour, M.M.: Differential transform vibration and modal stress analyses of circular plates made of two-directional functionally graded materials resting on elastic foundations. Arch. Appl. Mech. **81**, 1289–1306 (2011)
12. Rahmati Nezhad, Y., Asemi, K., Akhlaghi, M.: Transient solution of temperature field in functionally graded hollow cylinder with finite length using multi layered approach. Int. J. Mech. Mater. Des. **7**, 71–82 (2011)
13. Shao, Z.S.: Mechanical and thermal stresses of a functionally graded circular hollow cylinder with finite length. Int. J. Press. Vessel. Pip. **82**, 155–163 (2005)
14. Elishakoff, I., Gentilini, C., Viola, E.: Three-dimensional analysis of an all-round clamped plate made of functionally graded materials. Acta Mech. **180**, 21–36 (2005)
15. Liu, C.F., Lee, Y.T.: Finite element analysis of three-dimensional vibrations of thick circular and annular plates. J. Sound. Vib. **233**, 63–80 (2000)
16. Ashrafi, H., Bahadori, M.R., Shariyat, M.: Two-dimensional modeling of functionally graded viscoelastic materials using a boundary element approach. Adv. Mater. Res. **464**, 570–574 (2012)
17. Cheng, Z.Q., Batra, R.C.: Three-dimensional thermoelastic deformations of a functionally graded elliptic plate. Compos. Part B **31**, 97–106 (2000)
18. Prasad, K.L., Rao, A.V., Rao, B.N.: Free vibration of simply supported and clamped elliptical plates. J. Sound Vib. **158**, 383–386 (1992)
19. Wang, C.M., Wang, L., Liew, K.M.: Vibration and buckling of super elliptical plates. J. Sound Vib. **171**, 301–314 (1994)
20. Lim, C.W., Kitipornchai, S., Liew, K.M.: A free-vibration analysis of doubly connected super-elliptical laminated composite plates. Compos. Sci. Technol. **58**, 435–445 (1998)
21. Laura, P.A.A., Gutiérrez, R.H., Romanelli, E.: Transverse vibrations of a thin elliptical plate with a concentric, circular free edge hole. J. Sound Vib. **246**, 737–740 (2001)
22. Romashchenko, V.A., Storozhuk, V.N.: Theoretical analysis of strong changes in the shape of initially elliptic plates. Strength Mater. **34**, 54–61 (2002)
23. Altekin, M., Altay, G.: Static analysis of point-supported super-elliptical plates. Arch. Appl. Mech. **78**, 259–266 (2008)
24. Nallim, L.G., Grossi, R.O.: Natural frequencies of symmetrically laminated elliptical and circular plates. Int. J. Mech. Sci. **50**, 1153–1167 (2008)
25. Yüce, H., Wang, C.Y.: Perturbation methods for moderately elliptical plates with a core. Acta Mech. **215**, 105–114 (2010)
26. Lee, Z.Y., Chen, C.K., Hung, C.I.: Upper and lower bounds of the solution for an elliptic plate problem using a genetic algorithm. Acta Mech. **157**, 201–212 (2002)
27. Hsieh, J.-J., Lee, L.-T.: An inverse problem for a functionally graded elliptical plate with large deflection and slightly disturbed boundary. Int. J. Solids Struct. **43**, 5981–5993 (2006)
28. Chakraverty, S., Jindal, R., Agarwal, V.K.: Effect of non-homogeneity on natural frequencies of vibration of elliptic plates. Meccanica **42**, 585–599 (2007)
29. Ceribasi, S., Altay, G., Dokmeci, M.C.: Static analysis of super elliptical clamped plates by Galerkin's method. Thin-Walled Struct. **46**, 122–127 (2008)

30. Tang, H.-W., Yang, Y.-T., Chen, C.-K.: Application of new double side approach method to the solution of super-elliptical plate problems. Acta Mech. **223**, 745–753 (2012)
31. Ceribasi, S.: Static and dynamic analyses of thin uniformly loaded super elliptical FGM plates. Mech. Adv. Mater. Struct. **19**, 323–335 (2012)
32. Reddy, J.N.: Analysis of functionally graded plates. Int. J. Numer. Methods Eng. **47**, 663–684 (2000)
33. Croce, L.D., Venini, P.: Finite elements for functionally graded Reissner–Mindlin plates. Comput. Methods Appl. Mech. Eng. **193**, 705–725 (2004)
34. Mechab, I., Atmane, H.A., Tounsi, A., Belhadj, H.A., Adda Bedia, E.A.: A two variable refined plate theory for the bending analysis of functionally graded plates. Acta Mechanica Sinica **26**, 941–949 (2010)
35. Orakdogen, E., Kucukarslan, S., Sofiyev, A., Omurtag, M.H.: Finite element analysis of functionally graded plates for coupling effect of extension and bending. Meccanica **45**, 63–72 (2010)
36. Nguyen-Xuan, H., Tran, L.V., Thai, C.H., Nguyen-Thoi, T.: Analysis of functionally graded plates by an efficient finite element method with node-based strain smoothing. Thin-Walled Struct. **54**, 1–18 (2012)
37. Kim, J.H., Paulino, G.H.: Isoparametric graded finite elements for nonhomogeneous isotropic and orthotropic materials. J. Appl. Mech. **69**, 502–514 (2002)
38. Zhang, Z., Paulino, G.H.: Wave propagation and dynamic analysis of smoothly graded heterogeneous continua using graded finite elements. Int. J. Solids Struct. **44**, 3601–3626 (2007)
39. Ashrafi, H., Asemi, K., Shariyat, M., Salehi, M.: Two-dimensional modeling of heterogeneous structures using graded finite element and boundary element methods. Meccanica (2012). doi:10.1007/s11012-012-9623-5
40. Mori, T., Tanaka, K.: Average stress in matrix and average elastic energy of materials with misfitting inclusions. Acta Metall. **21**, 571–574 (1973)
41. Zienkiewicz, O.C., Taylor, R.L.: The Finite Element Method for Solid and Structural Mechanics. Elsevier, Oxford (2005)